Available online at www.sciencedirect.com
SCIENCE DIRECT®
Journal of Catalysis 219 (2003) 352–361
JOURNAL OF CATALYSIS
www.elsevier.com/locate/jcat

Characterization of Ga/HZSM-5 and Ga/HMOR synthesized by chemical vapor deposition of trimethylgallium

M. García-Sánchez, P.C.M.M. Magusin,* E.J.M. Hensen, P.C. Thüne, X. Rozanska, and R.A. van Santen

Schuit Institute of Catalysis, Eindhoven University of Technology, PO Box 513, 5600 MB Eindhoven, The Netherlands

Received 22 January 2003; revised 29 April 2003; accepted 1 May 2003

Abstract

Chemical vapor deposition (CVD) of trimethylgallium (TMG) has been studied as a method to disperse extraframework Ga in acidic ZSM-5 and mordenite zeolite. Various samples were extensively characterized by ICP, XPS, NMR, and FTIR. Silylation with tetramethyldisilazane is explored as a method for deactivating the external zeolite surface. The deposition of TMG in silylated ZSM-5 results in a gallium-to-aluminum ratio close to unity, which indicates a homogeneous metal distribution in the micropore space. However, pore blockage in the one-dimensional channels of mordenite results in a inhomogeneous distribution and a low Ga loading. Upon exposure to moistened air, the adsorbed methylgallium species decompose and alkoxy groups are formed. Subsequent oxidation or reduction leads to the complete removal of methyl groups. The reductive route is the preferred one resulting in a better dispersion of Ga, since oxidation of the methyl groups leads to water formation and hydrolysis of cationic Ga species.

Keywords: Zeolite; Gallium; ZSM-5; Mordenite; Trimethylgallium; Silylation; ^{71}Ga MAS NMR

1. Introduction

The mechanism for the dehydrogenation of small alkanes, one of the basic steps in their aromatization, over Ga/HZSM-5 catalyst has received a great deal of attention during the past decades [1–6]. These materials are presently used in the Cyclar process developed by British Petroleum and UOP [7]. The main reaction steps of this process are paraffin dehydrogenation followed by oligomerization and cyclization. Although relevant progress in the understanding of dehydrogenation reactions over zeolites containing Ga has been made in recent years, the role of the gallium species is still unclear. Some groups claim that the metal cations and acid sites play separate roles for alkane activation and cyclization [8–10]. Other authors argue that there is a synergistic effect where acid sites stabilize adsorbed alkanes and cleave C–H bonds while gallium facilitates the recombination of H atoms [1,11–13]. Various preparation methods have been described by which extraframework gallium can be incorporated into the micropores of HZSM-5: ion exchange in aqueous solution [4,14], impregnation [15], chemical vapor deposition (CVD) of $GaCl_3$ [16] and by physical admixture of Ga_2O_3 [17] or $GaCl_3$ [5]. It is also possible to obtain isomorphous substitution of aluminum by gallium in MFI-type zeolites by steam activation [18]. With aqueous ion exchange the hydrated Ga cations tend to stay on the external zeolite surface, and subsequent reduction or oxidation of the Ga species is necessary to disperse them into the micropores [6,17]. Sublimation of $GaCl_3$ is a more efficient method for depositing cationic Ga species directly into the micropores replacing Brønsted acid sites [16,19]. However, the subsequent treatment with water necessary to remove chlorine causes the hydrolysis of Ga atoms and the regeneration of some Brønsted acid sites [16]. As an alternative route, we here address a completely anhydrous procedure consisting of chemical vapor deposition of trimethylgallium (TMG) with subsequent removal of the methyl groups by treatment with H_2 or O_2. Expectedly, the absence of water in our procedure prevents the formation of less-defined gallium (hydr)oxide species. Prior to a report of the catalytic activity, in this contribution we focus on the synthesis procedure and a detailed spectroscopic characterization of the

* Corresponding author.
E-mail address: p.c.m.m.magusin@tue.nl (P.C.M.M. Magusin).

0021-9517/$ – see front matter
doi:10.1016/S0021-9517(03)00231-8

resulting Ga zeolites. Three main aspects will be discussed: (i) the chemisorption and stability of TMG on HZSM-5 and HMOR zeolites, (ii) the effect of oxidation and reduction treatments on these catalysts, and (iii) the effect of protecting silanol groups on the external surface by silylation before TMG deposition [20]. This latter aspect is important since TMG reacts with both silanol groups [21] and Brønsted acid sites [22], respectively, mainly located on the outer zeolite surface and in the zeolite pores. In catalytic applications, one generally aims to take advantage of the shape-selective effects of the small pore dimensions of zeolites. Preferably, the aim is to disperse the Ga species inside the zeolite pores. In order to prevent the undesirable reaction with silanol sites, we have tested the effect of blocking the silanol groups at the external zeolite surface by silylation with tetramethyldisilazane. This compound represents an effective silylating reagent to modifying the external surface through [23]

$$2{\equiv}\mathrm{SiOH} + \mathrm{HN}\begin{matrix}\diagup\ \mathrm{SiH(CH_3)_2}\\ \diagdown\ \mathrm{SiH(CH_3)_2}\end{matrix} \rightarrow 2{\equiv}\mathrm{SiO{-}Si}\begin{matrix}\diagup\ \mathrm{CH_3}\\ \text{—}\ \mathrm{H}\\ \diagdown\ \mathrm{CH_3}\end{matrix} + \mathrm{NH_3}. \quad (1)$$

TMG-loaded catalysts were prepared either from silylated or freshly calcined zeolites. These catalysts were extensively characterized by multinuclei NMR, FTIR, ICP-OES, and XPS. Special attention was paid to the development of the Ga species after hydrogen or oxygen treatments. In the course of our study, we have found that the adsorbed methylgallium species already reacts with air at ambient conditions. Therefore, we also paid attention to this first step.

2. Experimental

2.1. Catalysts synthesis

2.1.1. Chemical vapor deposition of TMG

HZSM-5 and HMOR were obtained by calcination of the parent zeolites NH_4ZSM-5 (Akzo Nobel, Si/Al = 19.4) and NH_4MOR (Akzo Nobel, Si/Al = 10). Ga/HZSM-5 and Ga/HMOR were prepared by chemical vapor deposition of trimethylgallium (Strem Chemicals, purity > 99%) on these acidic zeolites. The amount of 3.5 g of previously dried acidic zeolite was loaded in a reactor with an excess amount of TMG (1 ml) in an argon-flushed glovebox at room temperature. After 24 h, the resulting material was maintained under vacuum for 2 h to remove unreacted TMG and gaseous reaction products, mainly methane [24]. The catalysts were kept in Ar atmosphere prior to further use.

2.1.2. Silylation

The silanol groups in HZSM-5 and HMOR were silylated employing the procedure of Anwander and co-workers [23]. The silylated zeolites were obtained as follows: 3 g of tetramethyldisilazane was diluted in 30 ml of *n*-hexane and added to a 120 ml suspension of 3 g of dried zeolite in *n*-hexane. The solution was stirred for 24 h at ambient temperature. The mixture was filtrated and washed several times with *n*-hexane. Finally, the silylated materials were dried for 24 h at 383 K. The deposition of trimethylgallium on silylated zeolite followed the same procedure as outlined above.

2.2. Pretreatment

The resulting catalysts were either calcined in 100 ml/min of a mixture of 20 vol% O_2 in nitrogen or reduced in 100 ml/min of 20 vol% H_2 in nitrogen. These treatments were performed under the following heating program: 7 K/min to 523 K and 2 h isothermal followed by 7 K/min to 823 K and 4 h isothermal.

Catalysts are denoted as [TMG/] ZEO ([Sy], X), where TMG optionally indicates TMG deposition, ZEO stands for ZSM-5 or MOR, Sy indicates optional silylation, and X indicates either oxidative (O), reductive (R) treatment or hydrated with deoxygenated water (W). The latter treatment was obtained by exposing the fresh catalyst to a flow of deoxygenated water for 5 h. The deoxygenated water was produced after boiling distillate water for 1 h and flowing 100 ml/min of N_2 for 24 h. This treatment was applied prior to ^{13}C and ^{1}H NMR analysis to study the decomposition of TMG on zeolites. To analyze the simultaneous effect of oxygen and water, the fresh catalysts were simply exposed to moistened air for 24 h.

2.3. Characterization

Magic-angle-spinning (MAS) NMR spectra were recorded on a Bruker DMX500 spectrometer operating at 500.13 MHz for ^{1}H, 152.5 MHz for ^{71}Ga, and 125.76 MHz for ^{13}C nuclei. For ^{71}Ga MAS NMR, ∼ 10 mg hydrated zeolite was packed into a 2.5-mm sample holder and rotated at a rate of 30 kHz. To better characterize the broad ^{71}Ga resonances, whole Hahn echoes were recorded using a rotor-synchronized 90–τ–180 pulse sequence with a 90° pulse of 0.7 μs, a delay τ of 32.3 μs. Typically between 4000 and 25,000 scans were accumulated with a time resolution of 0.5 μs (1-MHz spectral width) and an interscan delay of 3 s. No spectral-intensity change was observed for a shorter interscan delay of 1 s. Solid $GaNO_3$ was used for external shift calibration, and Ga_2O_3 to optimize the pulse sequence. For ^{1}H and ^{13}C NMR experiments, we used 4-mm sample holders and a rotation rate of 8 kHz. Except when studying the effect of air, the samples were packed under argon atmosphere to prevent hydration. ^{1}H NMR spectra were recorded using single-pulse excitation with a 54° pulse of 3 μs. The number of scans was 16 and the interscan delay was 3 s. Ethanol with its proton signals at 5.0, 3.5, and 1.0 ppm was used as an external reference. ^{13}C NMR spectra were obtained using either ^{1}H–^{13}C varied-amplitude cross-polarization (VACP) with a contact time of 1 ms, or a rotor-synchronized 90–τ–180–τ pulse sequence with a 5 μs 90° pulse and a delay τ

of 117.5 μs. In both cases, 2048 scans were typically accumulated with an interscan delay of 5 s. No signal-intensity change was observed at a shorter interscan delay of 2 s. The 38.56 ppm signal of adamantane was used for external calibration. Two-dimensional (2D) ^{1}H–^{13}C NMR correlation experiments to improve the identification of hydrocarbon species were carried out with a varied-amplitude version of the wideline-separated (WISE) pulse sequence with a contact time of 1 ms [25]. The number of scans was 128, the number of experiments 200, and the interscan delay 5 s.

FTIR spectra were obtained in a Bruker IFS113V FT absorbance spectrometer with spectral recorded between 1000 and 400 cm^{-1}. In a typical experiment, the samples were evacuated at room temperature for 2 h. The catalysts were calcinated at 773 K or reduced at 673 K in situ for 60 min. All the IR spectra were recorded at room temperature.

The XPS measurements were done with a VG Escalab MKII spectrometer, equipped with a dual Al/Mg-K_α X-ray source. Spectra were obtained using the aluminum anode (Al-$K_\alpha = 1486.6$ eV) operating at 480 W and constant pass energy of 20 eV with a background pressure of 2×10^{-9} mbar.

The contents of Ga and Al were determined by inductively coupled plasma optical emission spectrometry (ICP-OES) technique, using a Spectro Ciros^{CCD} spectrometer.

All theoretical calculations have been performed with Gaussian98 [26]. We used the hybrid DFT B3LYP method [27–29]. In the case of zeolite systems, this method has been shown to give results as good as or better than MP2 calculations [30,31]. The basis set 6-311g** has been used for all atoms. The zeolite crystal is modeled by a small molecular fragment that aims to describe the sites of interest, viz. zeolite hydroxyl groups and acidic Brønsted site. Two zeolite cluster models have been used. First, an 18 atom cluster ($Si(OH)(OSiH_3)_3$) was employed to represent a silanol group Si–OH. Second, a Brønsted site model cluster was made up by 22 atoms ($Al(OSiH_3)_3(OHSiH_3)$) to represent a Al–O(H)–Si site. Geometry optimization calculations have been carried out to obtain a local minimum for reactants, adsorption complexes, and products. The frequencies were computed using analytical second derivatives for a temperature of 298 K. Zero-point energy (ZPE) corrections have been calculated for all optimized structures.

3. Results

3.1. Catalyst composition

The gallium loadings on the various samples are listed in Table 1. TMG/ZSM-5 has a higher gallium content than TMG/MOR although the Si/Al ratio of HZSM-5 is approximately two times higher than that of HMOR. From ICP analyzes after oxidative and reductive treatments, it follows that these treatments do not lead to a significant reduction of the Ga content of the samples. Samples prepared with silylated zeolites, TMG/ZSM-5(Sy) and TMG/MOR(Sy), contain approximately 30% less gallium than materials prepared with nonsilylated zeolites. This observation indicates that silylation of zeolites decreases the number of sites where TMG can adsorb. The Ga/Al ratio of TMG/ZSM-5(Sy) is close to unity.

Table 1
Gallium content, Ga/Al molar ratio (ICP), and Ga/Si molar ratio (XPS)

Sample	wt% Ga	Ga/Al	Ga/Si
TMG/ZSM-5	6.8	1.5	
TMG/ZSM-5(O)	6.4	1.5	
TMG/ZSM-5(R)	6.3	1.5	
TMG/MOR	3.4	0.4	0.34
TMG/MOR(O)	3.4	0.4	0.17
TMG/MOR(R)	3.1	0.4	0.04
TMG/ZSM-5(Sy)	5.0	1.1	
TMG/MOR(Sy)	2.3	0.3	0.17

3.2. XPS results and migration of Ga

Table 1 shows the Ga/Si ratios obtained by XPS. It is important to note that these values give an indication of the Ga/Si ratio at the outer surface of zeolites due to the limited mean free electron path (∼ 5 nm). Clearly, the surface region of TMG/MOR is enriched in Ga (Ga/Si = 0.34) compared to the cases where TMG/MOR has been oxidized or reduced. The decrease of the Ga/Si ratio measured by XPS after reduction or oxidation of catalysts indicates the migration of Ga present on the outer surface and its redistribution through the mordenite micropores. Adbul Hamid and co-workers [32] observed similar behavior for a Ga/HZSM-5 catalyst prepared by ion exchange with Ga–nitrate. Here, we stress that the amount of Ga observed by XPS constitutes only a very small fraction of the total Ga present in the catalyst.

3.3. ^{13}C CPMAS NMR spectroscopy

The chemisorption of TMG on both zeolites and its successive decomposition in contact with oxygen and water was analyzed by one- and two-dimensional ^{13}C and ^{1}H NMR.

Fig. 1 shows the ^{13}C NMR spectra of TMG chemisorbed on silylated and nonsilylated HZSM-5. As-prepared TMG/ZSM-5 before exposure to air or water presents a broad ^{13}C NMR signal at −7 ppm (Fig. 1a), which is assigned to Ga–CH_3 [33]. To obtain information about the stability of TMG dispersed in the ZSM-5 matrix, the as-prepared TMG/ZSM-5 was exposed to an argon flow containing oxygen (Fig. 1b), or deoxygenated water vapor (Fig. 1c) at room temperature. The resulting NMR spectra closely resemble those of the asprepared material. After exposure of TMG/ZSM-5 and TMG/ZSM-5(Sy) to moistened air, however, two new signals appear at 60 and 18 ppm (Figs. 1d and e). The signal at 60 ppm is assigned to $^{13}\underline{C}H_3$–O and/or CH_3–$^{13}\underline{C}H_2$–O, probably connected to Ga. However, the ^{13}C NMR shift

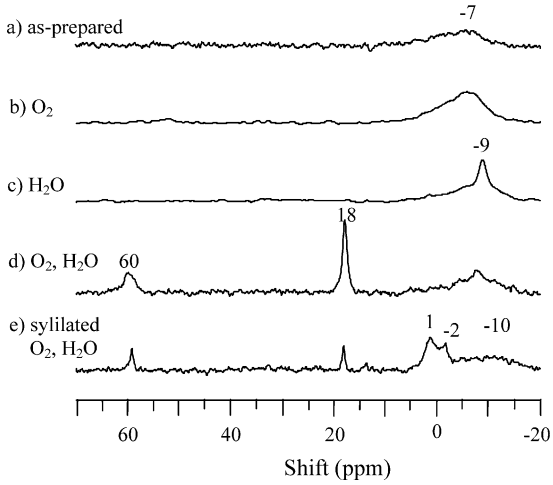

Fig. 1. ^{13}C NMR spectra of TMG/ZSM-5 after synthesized (a), exposed to O_2 (b), deoxygenated H_2O (c), exposed to moistened air (d), and TMG/ZSM-5(Sy) exposed to moistened air. The second and third spectra have been recorded with VACP, the other three with a Hahn–echo pulse sequence.

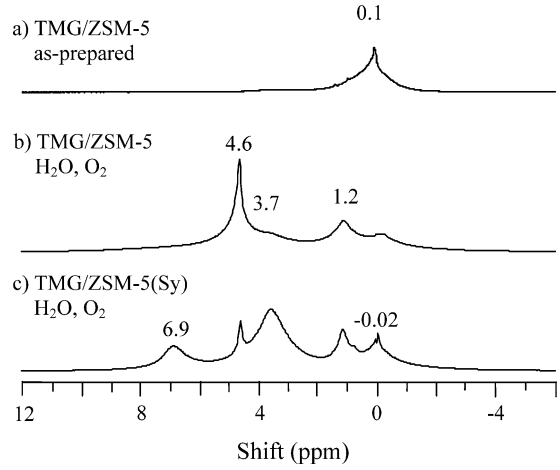

Fig. 2. ^1H NMR spectra of as-prepared TMG/ZSM-5 (a), TMG/ZSM-5 (b), and TMG/ZSM-5(Sy) (c) exposed to moistened air.

alone does not exclude a possible linkage of alkoxy groups to Si or Al. The signal at 18 ppm is assigned to a methyl group connected to another C atom [34–36]. The silylated TMG/ZSM-5(Sy) catalyst presents additional signals between 1 and −2 ppm (Fig. 1d). These are methyl signals, which probably arise from the trimethylsiloxy species generated in the silylation of the silanol groups [23]. The lineshape suggests a bimodal distribution of structures or environments.

3.4. ^1H NMR spectroscopy

^1H NMR experiments confirm the formation of methoxy and ethoxy groups after exposure to moistened air. The spectra of fresh TMG/ZSM-5 (Fig. 2a) consists of a single broad signal at 0.1 ppm assigned to Ga–CH_3. When the catalyst was exposed to moistened air, a new signal at 1.2 ppm appears, which belongs to methyl groups bonded to C atoms, like in an ethoxy groups. Both CH_3–O and –CH_2–O groups give rise to overlapping signal at 3.7 ppm. The signal at 4.6 ppm is due to water adsorbed on HZSM-5 [37].

The spectra obtained for TMG/ZSM-5(Sy) exposed to moistened air (Fig. 2c) show a relatively intensive signal at 3.7 ppm as compared to that in Fig. 2b, indicating an enhanced methoxy: ethoxy ratio for silylated catalysts. The signal at −0.02 ppm is assigned to methyl groups from the silylating reagent. The CH_3–Si–O signal probably overlaps with the Ga–CH_3 signal at 0.1 ppm. A new peak at 6.9 ppm is assigned to NH_4^+ produced during the silylation of zeolite that remains adsorbed after chemisorption of TMG [38].

3.5. Two-dimensional ^1H–^{13}C correlation NMR

^1H and ^{13}C NMR signals, which overlap in one-dimensional spectra, are generally better resolved in two-dimensional ^1H–^{13}C NMR spectra. The experiment is selective for ^{13}C nuclei with protons in their direct surroundings (< 1 nm). By correlating the ^1H and ^{13}C shifts, the chemical structure of the hydrocarbon species can be identified more specifically. Fig. 3 shows the 2D ^1H–^{13}C NMR spectra of the nonsilylated TMG/ZSM-5 catalyst after exposure to moistened air. For comparison, the spectral projections on the ^1H and ^{13}C axis are indicated, as well as the corresponding one-dimensional spectra. The spectrum confirms the formation of methoxy and ethoxy species and the presence of methyl groups that remain bonded to Ga or Si atoms in silylated zeolites. Note that the 4.6 ppm proton signal is absent in the 2D spectrum, as expected for a water signal.

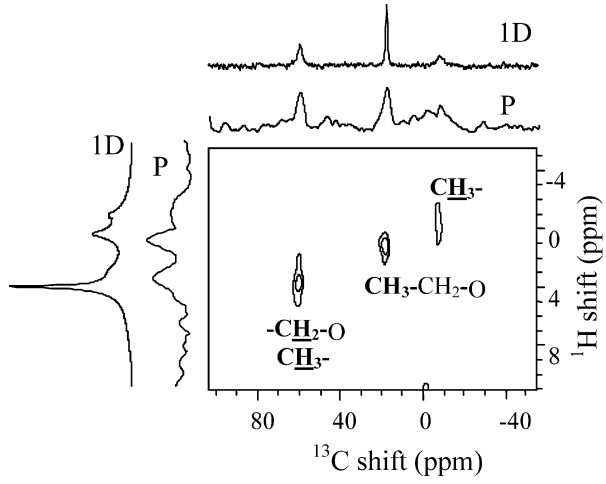

Fig. 3. 2D ^1H–^{13}C NMR spectra of TMG/ZSM-5 exposed to moistened air. Projections on the ^1H and ^{13}C axes are marked as "P." For comparison the corresponding one-dimensional spectra (Figs. 1d and 2b) have been added.

3.6. ^{71}Ga MAS NMR spectroscopy

Fig. 4a shows the ^{71}Ga MAS NMR spectra of the gallium(II)chloride used as model compound. In the solid gallium dichloride $Ga^+[Ga^{3+}Cl_4]$, the Ga^{3+} is at the center of

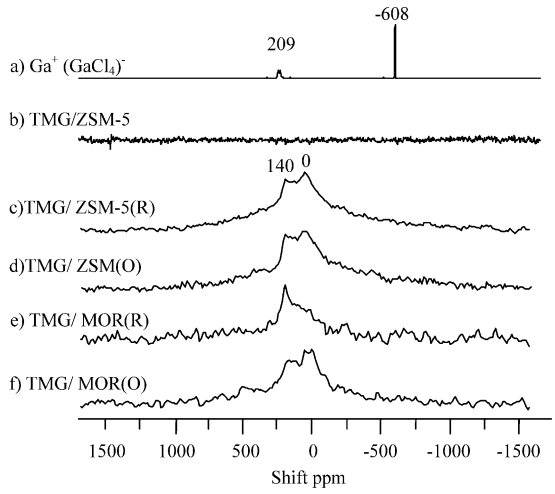

Fig. 4. 30-kHz magic-angle spinning ^{71}Ga MAS NMR spectrum of Ga_2Cl_4 (a), TMG/ZSM-5 as-prepared (b), reduced (c), and oxidized (d), TMG/MOR reduced (e) and oxidized (f).

a $GaCl_4$ tetrahedron, in which the bonds have considerable covalent character. Ga^+ forms longer and more ionic bonds with chlorine [39]. We ascribe the ^{71}Ga MAS NMR signals at 209 and −608 ppm to Ga^{3+} and Ga^+, respectively. The ^{71}Ga MAS NMR signals of as-prepared TMG/MOR and TMG/ZSM-5 catalysts were not visible, probably because of the low coordination symmetry around Ga that results in a huge quadrupolar line broadening (Fig. 4b). This is in line with an earlier study by Bayense and coworkers [18], who assumed that part of the gallium in dealuminated TMG/ZSM-5 catalyst is undetectable by NMR. Hydration of the zeolites to reduce the internal electric-field gradients and obtain a narrower ^{71}Ga signal was unsuccessful.

The H_2- or O_2-treated, and then air-exposed TMG/ZSM-5 and TMG/MOR catalysts have a visible, although extremely broad ^{71}Ga signal. Even with the ultrafast sample-rotation rate of 30-kHz applied in our experiments, we are unable to obtain well-resolved sideband patterns. The lineshape suggests a bimodal distribution of Ga species with shift values centered around 0 and 140 ppm. These two values are typical of trivalent Ga^{3+} with octahedral and tetrahedral oxygen coordination, respectively [40–42]. Note that the samples after H_2 or O_2 treatment were exposed to moistened air to narrow the ^{71}Ga MAS NMR signal, thus leading to the partial decomposition of TMG. TMG/ZSM-5(O) and TMG/ZSM-5(H) show similar ^{71}Ga MAS NMR spectra (Figs. 4c–d). In contrast, in TMG/MOR(H) (Fig. 4e) the signal at 140 ppm is relatively enhanced compared to TMG/MOR(O) (Fig. 4f).

3.7. FTIR studies

The IR spectra of freshly calcined HZSM-5 and TMG/ZSM-5 after oxidative and reductive treatment are displayed in Fig. 5. Three bands due to OH stretching vibrations were identified for the parent HZSM-5 zeolite (Fig. 5a). These bands are assigned as follows: 3612 cm^{-1} for Brønsted acid sites, 3664 cm^{-1} for extralattice AlOH ions, and 3744 cm^{-1} for terminal silanol groups [43]. The extraframework Al ions are already present in the as-received material and arise from the synthesis procedure. The signal of Brønsted acid sites is hardly distinguishable for as-prepared TMG/ZSM-5 (Fig. 5b). A new broad band appears, indicating the presence of water adsorbed during sample preparation for IR measurement. Nonetheless, the signal of silanol sites is not present anymore. Signals at 2924 and 2981 cm^{-1} belong to the asymmetric C–H stretching of methyl groups or methane adsorbed on ZSM-5 [44–46]. These bands disappear after oxidation or reduction of the TMG/ZSM-5 catalyst (Figs. 5c–d), indicating the complete decomposition of those groups. Whereas in TMG/ZSM-5(R) no bridging hydroxyl groups are observed, an oxidative treatment (TMG/ZSM-5(O)) results in a small number of Brønsted protons. The band at 3664 cm^{-1} in the parent sample corresponds to extralattice AlOH species. In TMG/ZSM-5(O), a more dominant band at 3672 cm^{-1} is observed that most probably corresponds to extralattice GaOH groups. These OH groups could derive from water produced during oxidation of the alkyl groups. Furthermore, this water may induce a small amount of dealumination of the zeolite structure as was readily observed from ^{27}Al NMR measurements (not shown here). Water production also explains the small amount of Brønsted protons regenerated due to hydrolysis of charge-compensating Ga cations. However, we surmise that most of the negative zeolite charge is compensated by Ga-containing cationic species.

In Fig. 6, the FTIR results of the silylated samples are collected. Figs. 6b and c show the spectra of silylated HZSM-5 after oxidation and reduction, ZSM-5(Sy,O) and ZSM-5(Sy,R). Comparing these two spectra with the parent HZSM-5 (Fig. 6a), we observe that the signal of silanol groups at 3743 cm^{-1} is strongly decreased. The

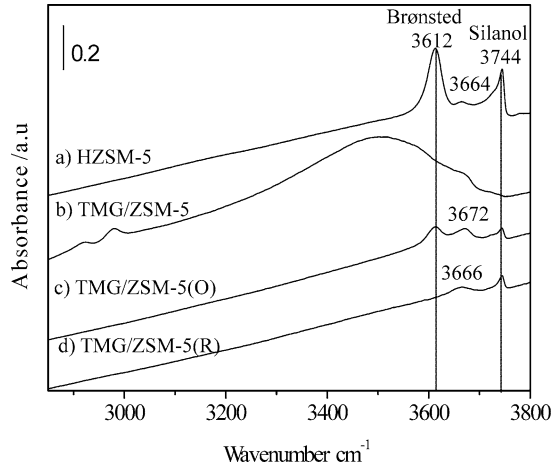

Fig. 5. FTIR spectra of HZSM-5 (a), TMG/ZSM-5 exposed to moistened air (b), after oxidation in situ (c) and after reduction in situ (d).

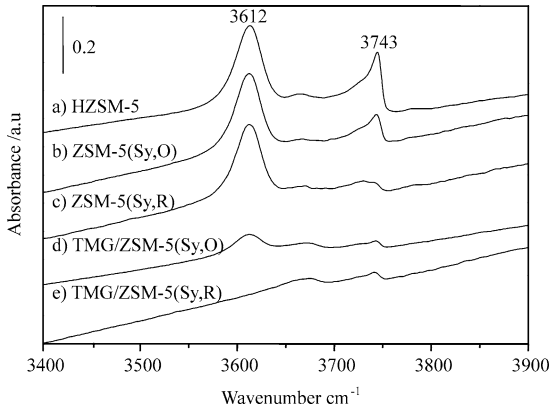

Fig. 6. FTIR spectra of HZSM-5 (a); silylated HZSM-5 after oxidation (b), and after reduction (c); TMG chemisorbed on silylated HZSM-5 after oxidation (d) and after reduction (e).

peak corresponding to Brønsted acid sites (3612 cm^{-1}) is not significantly altered, indicating that the silylating agent has selectively reacted with silanol groups. The spectra of TMG/ZSM-5(Sy,O) and TMG/ZSM-5(Sy,R) show a drastic decrease of this signal after chemisorption of TMG (Figs. 6d and e). Similar to the nonsylilated samples, it is observed that the signal corresponding to Brønsted acid sites completely disappears after reduction.

3.8. Theoretical modeling

Theoretical calculations were performed to estimate the energy of the reaction of trimethylgallium or tetramethyldisilazane with the silanol groups or Brønsted acid sites. The adsorption of $Ga(CH_3)_3$ on acid zeolites may lead to the formation of methane and chemisorbed $Ga(CH_3)_2{}^+$ cations according to

Silanol site:

$$\equiv Si\text{–}OH + Ga(CH_3)_3 \rightarrow \equiv Si\text{–}O\text{–}Ga(CH_3)_2 + CH_4; \qquad (2)$$

Brønsted site:

$$\equiv Al\text{–}O(H)\text{–}Si\equiv + Ga(CH_3)_3 \rightarrow \equiv Al\text{–}O(Ga(CH_3)_2)\text{–}Si\equiv + CH_4. \qquad (3)$$

Table 2 shows the computed thermochemical data of these reactions. Chemisorption on Brønsted sites is thermodynamically more favorable than on silanol sites. Geometric optimization analysis indicated that the most stable structure is the one where $Ga(CH_3)_2{}^+$ is tetrahedrally coordinated to two framework oxygen atoms (Fig. 7). The reaction of TMG and terminal silanol sites results in interaction with an oxygen atom which is less favorable (Fig. 8). In general, one should also consider the possibility of TMG reacting with two neighboring hydroxyl groups giving monomethylgallium. The probability for the occurrence of two aluminum-containing oxygen tetrahedral in mordenite ($Si/Al = 10$) is significantly higher than in ZSM-5 ($Si/Al = 19.4$).

Table 2
Computed thermodynamic data (energies in kJ/mol) of the reaction between TMG and zeolite hydroxyl groups

	Silanol group (2)	Brønsted acid site (3)
$\Delta H_r^{298\,K}$	−121.8	−203.4
$\Delta G_r^{298\,K}$	−102.5	−203.9
$\Delta H_r^{0\,K}$	−122	−209

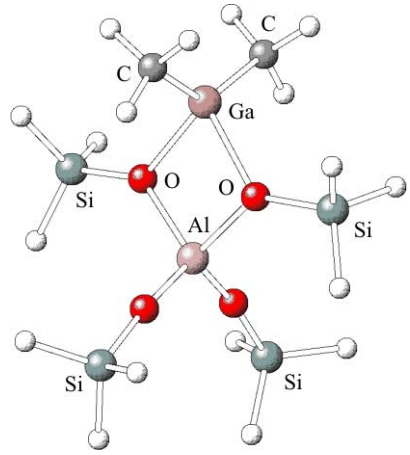

Fig. 7. Schematic representation of trimethylgallium chemisorbed on Brønsted acid sites.

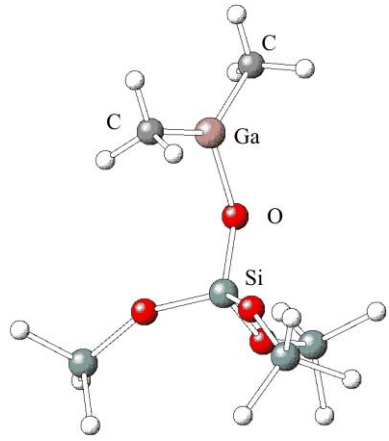

Fig. 8. Schematic representation of trimethylgallium chemisorbed on silanol sites.

Silylation of the parent zeolite with $NH(SiH(CH_3)_2)_2$ involves a double protonation of the nitrogen atoms. The zeolite protons are replaced by $–SiH(CH_3)_2$ groups and NH_3 is released. The silylation of silanol and Brønsted sites probably proceeds in two steps, on silanol sites as

$$\equiv Si\text{–}OH + NH(SiH(CH_3)_2)_2 \rightarrow \equiv Si\text{–}O\text{–}SiH(CH_3)_2 + NH_2(SiH(CH_3)_2), \qquad (4a)$$

$$\equiv Si\text{–}OH + NH_2(SiH(CH_3)_2) \rightarrow \equiv Si\text{–}O\text{–}SiH(CH_3)_2 + NH_3, \qquad (4b)$$

Table 3
Computed thermodynamic data (energies in kJ/mol) of the reaction between $NH(SiH(CH_3)_2)_2$, $NH_2SiH(CH_3)_2$ and zeolite hydroxyl groups

	Silanol group		Brønsted acid site	
	(4a)	(4b)	(5a)	(5b)
$\Delta H_r^{298\,K}$	−60.5	−59.8	−42.9	−42.1
$\Delta G_r^{298\,K}$	−56.1	−54.5	−31.4	−29.9
$\Delta H_r^{0\,K}$	−58	−62	−41	−45

and on Brønsted sites as

$$\equiv Al–O(H)–Si\equiv + NH(SiH(CH_3)_2)_2 \rightarrow \equiv Al–O(SiH(CH_3)_2)–Si\equiv + NH_2(SiH(CH_3)_2), \quad (5a)$$

$$\equiv Al–O(H)–Si\equiv + NH_2(SiH(CH_3)_2) \rightarrow \equiv Al–O(SiH(CH_3)_2)–Si\equiv + NH_3. \quad (5b)$$

The thermodynamic data indicate that the silylated silanol groups are more stable than the silylated Brønsted acid sites (Table 3). Thus, from a thermodynamic point of view, there is a preference for silylation of the silanol groups.

4. Discussion

4.1. Chemical vapor deposition of trimethylgallium

Comparing TMG/ZSM-5 and TMG/MOR we observe that the mordenite-based samples have a considerably lower Ga content (Table 1). The average Ga/Al ratio for the ZSM-5-based catalysts is higher than unity, indicating that TMG reacts with both Brønsted acid sites and silanol groups. In TMG/ZSM-5(Sy) the Ga/Al ratio is close to unity. This is interpreted as a selective reaction of TMG with the acidic protons due to the protection of the silanol groups by silylation. The lower Ga content of TMG/MOR is most likely related to the one-dimensional pore system of mordenite. In effect, chemisorption of TMG in the zeolite pores close to the pore entrances prevents further diffusion of TMG throughout the micropores. Thus, mordenite-based catalysts have an initial outer surface enriched in Ga. The more accessible structure of ZSM-5 results in a homogeneous distribution of Ga over all the Brønsted acid sites.

FTIR spectra show that chemisorption of TMG modifies the hydroxyl bands of ZSM-5 (Figs. 5a and b). Clearly, the silanol groups (3744 cm^{-1}) have disappeared. The signal of the bridging hydroxyl groups is overlapped by the broad absorption band of water. New bands around 2900–3000 cm^{-1} indicate the presence of methyl groups [44–46]. The adsorption of $Ga(CH_3)_3$ on HZSM-5 is accompanied by the formation of methane, $Ga(CH_3)_2{}^+$, and $Ga(CH_3)^{2+}$ ions [24]. The loss of protons from the Brønsted and silanol sites occurs concomitant with the formation of methane. The resulting $Ga(CH_3)_2{}^+$ and $Ga(CH_3)^{2+}$ ions are adsorbed on the negatively charged oxygen atoms and replace protons from the zeolite framework structure. These Ga ions exhibit a low coordination symmetry giving rise to a huge quadrupolar splitting and a broad ^{71}Ga MAS NMR signal (Fig. 4b).

Theoretical calculations indicate that chemisorption of TMG on Brønsted sites is thermodynamically more favorable than on silanol sites (Table 2). Nevertheless, FTIR results clearly pointed out that TMG reacts with both silanol and Brønsted acid sites (Figs. 5a and b). This is due to the excess of TMG and the more accessible positions of the silanol groups, which are mainly located on the external surface of the zeolite crystallites. The most stable structure is the one where $Ga(CH_3)_2{}^+$ is chemisorbed on a Brønsted site and coordinates to two oxygen neighbors of aluminum. Similar coordination was proposed by Gonzales and coworkers [47] for Ga/ZSM-5 catalysts treated with H_2. The divalent monomethyl Ga species, $Ga(CH_3)^{2+}$, prefers to simultaneously interact with two Brønsted sites, if these are sufficiently close together. This is more probable in the low-silica mordenite sample. When $Ga(CH_3)_3$ is chemisorbed on terminal silanol sites, Ga is connected to only one oxygen (Fig. 8).

Optimal Ga/ZSM5 catalysts for aromatization of alkanes are prepared by reduction with H_2 to disperse the gallium species. Chemisorption of TMG is selective to Brønsted acid sites resulting in a high dispersion of Ga species before reductive treatment.

4.2. Stability of chemisorbed TMG

Trialkylgallium compounds are unstable upon contact with water resulting in the hydrolysis of the alkane group and metal hydroxide. The reaction of trialkylgallium compounds and oxygen yields alkoxide compounds via alkylperoxo intermediates [48]. In order to obtain information about the stability of this compound on HZSM-5, as-prepared TMG/ZSM-5 was exposed to oxidative and reductive atmospheres and subsequently characterized by ^1H, ^{13}C, and 2D ^1H–^{13}C NMR. Methoxy and ethoxy groups are formed when TMG/ZSM-5 and TMG/ZSM-5(Sy) are exposed to water and oxygen simultaneously. ^1H and ^{13}C NMR spectra indicate the formation of alkoxy groups (Figs. 1d and e and 2b and c). To unequivocally prove the formation of alkoxy compounds and to avoid the overlapping signals from water, 2D ^1H–^{13}C NMR spectra were recorded to selectively detect the protons connected to carbons (Fig. 3). The resulting three signals are due to methyl groups in CH_3–Ga, CH_3–CH_2–O, and overlapping signals of CH_3–O and –CH_2–O species. Moreover, the FTIR bands around 2300–2900 cm^{-1} point to the presence of methyl groups in the samples that have been exposed to air (Fig. 5b). However, no formation of these methoxy and ethoxy species was observed when TMG/ZSM-5 was separately exposed to either deoxygenated water or oxygen. In this case, ^{13}C NMR spectra do not present additional signals next to the broad band assigned to methyl groups connected to Ga (Figs. 1b and c). TMG/ZSM-5(Sy) shows a similar stability in air. The ^{13}C

NMR spectra present the same bands assigned to alkoxy groups (Fig. 1e). Additional signals at 1.2 and −1.7 ppm are probably due to methyl groups from the silylating reagent.

In brief, the samples are unstable upon contact with moistened air at room temperature. Water and oxygen promote the hydroxylation of adsorbed $Ga(CH_3)_x$ species and the subsequent formation of alkoxy groups in silylated and nonsilylated HZSM-5. We assume that alkoxy groups are connected to Ga atoms. However, we are not able to distinguish by ^{1}H and ^{13}C NMR whether alkoxy groups are bonded to the Ga atoms or to the zeolite structure.

4.3. Silylation of zeolites

Silylation by tetramethyldisilazane is explored as a method to selectively deactivate silanol groups on the external surface. FTIR results of silylated HZSM-5 show a substantial decrease of the silanol site signal after oxidation or reduction, whereas the Brønsted signal is only slightly decreased (Figs. 6a–c). These results indicate that tetramethyldisilazane mainly reacts with silanol acid sites. Most of the Brønsted sites thus remain accessible for subsequent reaction with TMG.

Theoretical calculations predict that the interaction of tetramethyldisilazane with silanol groups is more favorable than that with Brønsted protons (Table 3). In addition, we surmise that the size of the silylating agent, which prevents diffusion into the micropores, is of overriding importance. The effectiveness of the silylation procedure is underlined by the lower Ga contents of the samples after deposition of TMG (Table 1). Moreover, for silylated ZSM-5 the resulting Ga/Al ratio is close to unity, indicating the direct deposition of one TMG molecule on one Brønsted acid site. The Ga content of the mordenite-based sample is also lower after silylation, although the overall Ga/Al ratios are much lower than unity. ^{1}H NMR spectra point to the presence of NH_4^+ ions produced during the silylation and adsorbed on the zeolite external surface (Fig. 2c) [38].

We conclude that silylation by tetramethyldisilazane is an effective method to deactivate the silanol groups on the external zeolite surface. Subsequent deposition of TMG results in a homogeneous distribution of Ga in the micropore space for ZSM-5. This distribution is less effective for mordenite due to diffusive limitations.

4.4. Oxidative and reductive treatments

The activation of the as-prepared Ga-containing zeolites is relevant to catalysis. We have examined the structure of Ga species after oxidative and reductive treatments. First of all, we note that there is hardly any loss of Ga during these treatments (Table 1). The nonideal Ga dispersion in the mordenite case can be alleviated by these oxidative and reductive treatments leading to the redispersion of Ga throughout the micropore space. This redispersion is confirmed by the decrease in the Ga/Si XPS ratio of mordenite catalyst. Especially, reductive treatments appear to be efficient in line with earlier observations [14,17,32]. However, the amount of Ga deposited is too low to cover all the acid sites.

From our extensive ^{13}C and ^{1}H NMR studies, we obtain the picture that due to air exposure the Ga species are hydroxylated and alkoxy groups are generated. These alkoxy groups are also observed by their IR signals between 2900 and 3000 cm^{-1} (Fig. 5b) [44,45]. These signals completely disappear after oxidative and reductive treatments, indicating the complete removal of these groups (Fig. 5c and d). Moreover, we find that for TMG/ZSM-5(Sy,O) and TMG/ZSM-5(O) almost all bridging hydroxyl groups have disappeared, while they are completely absent in the corresponding reduced samples. We surmise that the difference is mainly caused by water generated by the oxidation of the remaining alkyl groups in the case of oxidative treatment. This water may lead to the hydrolysis of Ga-containing cationic species and regeneration of a small part of acid protons. Additionally, this may lead to dealumination, although from ^{27}Al NMR measurements (not shown here) we conclude that its extent is quite low. The generation of protons due to hydrolysis leads to the formation of neutral Ga-oxo species in the zeolite micropores or at the external zeolite surface. Most probably, $[GaO]^+$ ions react with water according to

$$[GaO]^+ + H_2O \rightarrow GaO(OH) + H^+. \quad (6)$$

The subsequent decomposition of the GaO(OH) species could result in formation of gallium oxide clusters

$$2GaO(OH) \rightarrow Ga_2O_3 + H_2O. \quad (7)$$

The IR spectrum of HZSM-5 contains a band at 3664 cm^{-1} due to extraframework AlOH species, whereas the spectrum of TMG/ZSM-5 catalyst after oxidation exhibits a more intensive signal at 3672 cm^{-1} (Figs. 5a and c). This points to the presence of hydroxyl groups connected to extraframework Ga-oxide species as forwarded in (6). However, the relatively low amount of bridging hydroxyl groups after oxidation (FTIR) indicates that the amount of neutral Ga-oxide species should be quite low.

The interpretation of the ^{71}Ga NMR signals after oxidation and reduction and air exposure is more difficult (Fig. 4). Most importantly, we find that Ga is present as Ga^{3+} in two different coordinations. The resonance at 0 ppm is close to the one observed for Ga^{3+} in octahedral coordination in β-Ga_2O_3 [49]. The broad signal at 140 ppm is related to Ga^{3+} species in a lower than octahedral coordination symmetry. A resonance around 160 ppm has been detected when Ga is part of the zeolite framework structure in tetrahedral coordination [18,38,40,41]. In our case, the resonance at 140 ppm is likely due to tetrahedrally coordinated Ga^{3+} species such as $Ga(OH)_2^+$ coordinating to the Brønsted site. Additionally, a small fraction of Ga may be incorporated in the framework since the initial ZSM-5 structure possibly contains some defect sites. TMG/ZSM-5(R) and TMG/ZSM-5(O) show similar ^{71}Ga MAS NMR

spectra with broad overlapping signals (Figs. 4c and d). In contrast, TMG/MOR(R) shows a more intense signal at 140 ppm (Figs. 4e and f). Although not totally clear, this might relate to less water adsorption during air exposure in mordenite leading to a smaller extent of hydrolysis of charge-compensating species. Although these results clearly point to the presence of Ga^{3+}, one cannot rule out that Ga^{1+} may be present under reductive conditions at high temperature. Previous studies have indeed shown that upon cooling in H_2 the reduced Ga/HZSM-5 to room temperature Ga^{1+} is oxidized to Ga^{3+} [13]. Moreover, our samples were exposed to air prior to NMR measurements. Finally, we note that similar results were obtained after oxidation and reduction for the silylated zeolites. At present, a catalytic study is underway to compare hydrocarbon activation of these catalysts to those prepared by conventional impregnation of Ga–nitrate or vapor deposition of $GaCl_3$ followed by hydrolysis.

5. Conclusions

Chemical vapor deposition of trimethylgallium followed by H_2 treatment to remove the remaining methyl groups is an efficient method to disperse Ga in the micropore space of acid zeolites. Silylation with tetramethyldisilazane is effective in deactivating the silanol groups on the external zeolite surface. While deposition of trimethylgallium on silylated HZSM-5 leads to a homogeneous distribution of the Ga species with a Ga/Al ratio close to unity, the lower dimensionality of the mordenite framework results in pore blockage during deposition and Ga/Al ratios lower than unity. The reaction of chemisorbed TMG with moistened air was studied in more detail. In the presence of both O_2 and H_2O, oxygen inserts into Ga–C bonds resulting in the formation of methoxy and, quite surpisingly, ethoxy groups. Hydrogen treatment is the preferable route for removing the remaining methyl groups, because the usual calcination leads to partial hydrolysis of the Ga cations from the Brønsted sites.

Acknowledgments

The authors thank to prof. V.B. Kazansky from the Zelinsky Institute of Organic Chemistry in Moscow, Russia, for fruitful discussions. We also thank Eugene van Oers for technical assistance during NMR measurements. One of us (MGS) acknowledges CONACyT (Mexico) for financial support.

References

[1] J.A. Biscardi, E. Iglesia, Catal. Today 31 (1996) 207.
[2] G. Buckles, G.J. Hutchings, Catal. Today 31 (1996) 233.
[3] V.I. Hart, M.B. Bryant, L.G. Butler, X. Wu, K.M. Dooley, Catal. Lett. 53 (1998) 111.
[4] B.S. Kwak, W.M.H. Sachtler, W.O. Haag, J. Catal. 149 (1994) 465.
[5] B.S. Kwak, W.M.H. Sachtler, J. Catal. 145 (1994) 456.
[6] A. Montes, G. Giannetto, Appl. Catal. A 197 (2000) 31.
[7] P.C. Doolan, P.R. Pujado, Hydrocarbon Process. 68–69 (1989) 72.
[8] H. Kitagawa, Y. Sendoda, Y. Ono, J. Catal. 101 (1986) 12.
[9] N.S. Gnep, J.Y. Doyemet, M. Guisnet, J. Mol. Catal. 45 (1988) 281.
[10] M. Guisnet, N.S. Gnep, F. Alario, Appl. Catal. A 89 (1992) 1.
[11] E. Iglesia, J.E. Baumgartner, G.L. Price, J. Catal. 134 (1992) 549.
[12] J. Yao, R. Le Van Mao, L. Dufresne, Appl. Catal. A 65 (1990) 175.
[13] G.D. Meitzner, E. Iglesia, J.E. Baumgartner, E.S. Huang, J. Catal. 140 (1993) 209.
[14] K.M. Dooley, C. Chang, G.L. Price, Appl. Catal. A 84 (1992) 17.
[15] V.R. Choudhary, K. Mantri, C. Sivadinarayana, Micropor. Mesopor. Mater. 37 (2000) 1.
[16] El.-M. El-Malki, R.A. van Santen, W.M.H. Sachtler, J. Phys. Chem. B 103 (1999) 4611.
[17] G. Price, V. Kanazirev, J. Catal. 126 (1990) 267.
[18] C.R. Bayense, J.H.C. van Hoof, J.W. de Haan, L.J.M. van de Ven, A.P.M. Kentgens, Catal. Lett. 17 (1993) 349.
[19] B.S. Kwak, W.M.H. Sachtler, J. Catal. 141 (1993) 729.
[20] C.T. O'Connor, K.P. Möller, H. Manstein, CATTECH 5 (2001) 172.
[21] B.A. Morrow, R.A. McFarlane, J. Phys. Chem. 90 (1986) 3192.
[22] M.W. Anderson, G.K. Logothetis, M.E. Pemble, A.G. Taylor, N.C. Wallace, H.M. Yates, Adv. Mater. Opt. Electron. 2 (1993) 313.
[23] R. Anwander, I. Nagl, M. Widenmeyer, J. Phys. Chem. B. 104 (2000) 3532.
[24] U. Seidel, M. Koch, E. Brunner, B. Staudte, H. Pfeifer, Micropor. Mesopor. Mater. 35–36 (2000) 341.
[25] J.D. Mao, B. Xing, K. Scmidt-Rohr, Environ. Sci. Technol. 35 (2001) 1928.
[26] M.J. Frisch, G.W. Trucks, H.B. Schlegel G.E. Scuseria, M.A. Robb, J.R. Cheeseman, V.G. Zakrzewski, J.A. Montgomery, R.E. Stratmann, J.C. Burant, S. Dapprich, J.M. Millam, A.D. Daniels, K.N. Kudin, M.C. Strain, O. Farkas, J. Tomasi, V. Barone, M. Cossi, R. Cammi, B. Mennucci, C. Pomelli, C. Adamo, S. Clifford, J. Ochterski, G.A. Petersson, P.Y. Ayala, Q. Cui, K. Morokuma, D.K. Malick, A.D. Rabuck, K.Raghavachari, J.B. Foresman, J.Cioslowski, J.V. Ortiz, B.B. Stefanov, G. Liu, A. Liashenko, P. Piskorz, I. Komaromi, R. Gomperts, R.L. Martin, D.J. Fox, T. Keith, M.A. Al-Laham, C.Y. Peng, A. Nanayakkara, C. Gonzales, M. Challacombe, P.M.W. Gill, B.G. Johnson, W. Chen, M.W. Wong, J.L. Andress, M. Head-Gordon, E.S. Replogle, J.A. Pople, Gaussian 98, revision A.1, Gaussian Inc., Pittsburg, PA, 1998.
[27] A.D. Becke, Phys. Rev. A 38 (1988) 3098.
[28] C. Lee, W. Yang, R.G. Parr, Phys. Rev. B 37 (1988) 785.
[29] A.D. Becke, J. Chem. Phys. 98 (1993) 5648.
[30] S.A. Zygmunt, R.M. Mueller, L.A. Curtiss, L.E. Iton, J. Mol. Struct. 430 (1998) 9.
[31] B. Civalleri, E. Garrone, P. Ugliengo, J. Phys. Chem. B 102 (1998) 2373.
[32] S.B. Adbul Hamid, E.G. Derouane, G. Demortier, J. Riga, M.A. Yarmo, Appl. Catal. A 108 (1994) 85.
[33] E.K. Styron, S.J. Schauer, C.H. Lake, C.L. Watkins, L.K. Krannich, J. Organomet. Chem. 585 (1999) 266.
[34] H. Schumann, M. Frick, B. Heymer, F. Girgsdies, J. Organomet. Chem. 512 (1999) 117.
[35] S.M. Campbell, X.Z. Jiang, R.F. Howe, Micropor. Mesopor. Mater. 29 (1999) 91.
[36] R.J. Correa, C.J.A. Mota, J. Am. Chem. Soc. 124 (2002) 3484.
[37] M. Hunger, D. Freude, H. Pfeifer, J. Chem. Soc. Faraday Trans. 87 (1991) 657.
[38] M. Seiler, U. Schenk, M. Hunger, Catal. Lett. 62 (1999) 139.
[39] A.F. Holleman, E. Wiberg, in: Inorganic Chemistry, Academic Press, New York, 1995, p. 1036.
[40] A.C. Wei, P.H. Liu, K.J. Chao, E. Yang, H.Y. Cheng, Micropor. Mesopor. Mater. 42 (2001) 147.

[41] C.R. Bayense, A.P.M. Kentgens, J.W. de Haan, L.J.M. van de Ven, J.H.C. van Hoof, J. Phys. Chem. 96 (1992) 775.
[42] A. Montes, Z. Gabélica, A. Rodríguez, G. Giannetto, Appl. Catal. A 169 (1998) 87.
[43] S. Kumar, A.K. Sinha, S.G. Hegde, S. Sivasanker, J. Mol. Catal. A 154 (2000) 115.
[44] R.L. Puurunen, A. Root, S. Haukka, E.I. Iiskola, M. Lindblad, A.O.I. Krause, J. Phys. Chem. B 104 (2000) 6599.
[45] T.R. Forester, R.F. Howe, J. Am. Chem. Soc. 109 (1987) 5076.
[46] X.Z. Jiang, J. Mol. Catal. A Chem. 121 (1997) 63.
[47] N.O. Gonzales, A.K. Chakraborty, A.T. Bell, Top. Catal. 9 (1999) 207.
[48] A.R. Barron, M.B. Power, in: R.B. King (Ed.), Encyclopedia of Inorganic Chemistry, Vol. 3, Wiley, Chichester, 1994, p. 1269.
[49] D. Massiot, I. Farnan, N. Gautier, D. Trumeau, A. Trokiner, J.P. Coutures, Solid State Nucl. Magn. Reson. 4 (1995) 241.